

# Chapter 3

## Excitation of Molecules in Intense, Ultrashort Laser Pulses

This chapter presents an overview of physical processes and phenomena which are important for the interpretation of experimental results of gas phase  $C_{60}$  interacting with high-intensity laser fields (up to  $10^{14}$  W/cm<sup>2</sup>).

Upon the absorption of energy, a molecular system is placed out of equilibrium. After energy is placed into the system, a reaction will occur to release the excess energy. For a free particle, there are three cooling mechanisms, ionization, fragmentation, and photon emission (fluorescence and phosphorescence). The timescales of these processes vary between molecular systems. In the present work, we are concerned with the decay mechanisms of ionization and fragmentation since the time scales that we are interested in, femtosecond to picosecond, the probability of photon emission is negligible.

The field of clusters in strong laser fields is still in its infancy. Many theoretical concepts of clusters in strong fields are still under development. The following will present the starting point of calculations and discuss several approximations.

### 3.1 Optical Excitation of Molecules

An incident laser's electric field excites the molecular system by introducing a time dependent potential in the system's Hamiltonian. Under the appropriate conditions, a photon can be absorbed by the molecule. The dynamics of the excitation can be described by the time-dependent Schrödinger equation. The solution of this equation gives the time-dependent wavefunction, which, in principle, can be related to all

properties of the system.

For a multi-atom and multi-electron system, the Hamiltonian is extremely complicated and the resulting time dependent Schrödinger equation has no analytical solution. The Hamiltonian can be expressed as

$$\begin{aligned}
 H(t) = & - \sum_{I=1}^N \frac{\hbar^2}{2m} \nabla_I^2 - \sum_{i=1}^M \frac{\hbar^2}{2m_e} \nabla_i^2 \\
 & + \frac{e^2}{4\pi\epsilon_0} \left[ - \sum_{I=1}^N \sum_{i=1}^M \frac{Z_I}{r_{iI}} + \sum_{i=1}^M \sum_{i<j=1}^M \frac{1}{r_{ij}} + \sum_{I=1}^N \sum_{I<J=1}^N \frac{Z_I Z_J}{r_{IJ}} \right] + H'(t) \quad (3.1)
 \end{aligned}$$

where capital letters indicate the nuclei and lower case letters indicate the electrons.  $m$  is the mass of the nuclei,  $m_e$  is the mass of the electron,  $N$  is the number of nuclei,  $Z$  is the charge of the nuclei (assumed to be the same),  $M$  is the number of electrons,  $r_{iI}$  is the separation of the  $i^{\text{th}}$  electron from the  $I^{\text{th}}$  nucleus,  $r_{ij}$  is the separation of the  $i^{\text{th}}$  and  $j^{\text{th}}$  electron, and  $r_{IJ}$  is the separation of the  $I^{\text{th}}$  and  $J^{\text{th}}$  nuclei.  $H'(t)$  is the time-dependent first order perturbation of the electric field, which in the dipole approximation can be expressed as

$$H'(t) = -\hat{\mu} \cdot \mathbf{E}(t) \cos \omega t \quad (3.2)$$

with  $\hat{\mu}$  the dipole operator and  $\mathbf{E}(t) \cos \omega t$  the time dependent electric field. The perturbation approach is frequently used in analysis of multiphoton processes [Fai87]. However, the perturbation theory is not appropriate to describe most of the interactions presented in this work since the intensity is generally bordering the multi-photon ionization and tunnelling regime.

The complexity of this problem necessitates approximations. The Born-Oppenheimer approximation allows for separation of the nuclear and electronic degrees of freedom and the kinetic energy of the nuclei can be neglected. By employing a jellium model, the positive charge of the nuclei is considered equally spread in space. This model is particularly good for describing large systems with delocalized electrons. The Hamiltonian (without perturbation) is thus far reduced to

$$H = - \sum_{i=1}^M \frac{\hbar^2}{2m_e} \nabla_i^2 + \sum_{i=1}^M \frac{\ell(\ell+1)}{2m_e r_i^2} + \frac{e^2}{4\pi\epsilon_0} \left[ - \sum_{i=1}^M \frac{Z}{r_i} + \sum_{i=1}^M \sum_{i<j=1}^M \frac{1}{r_{ij}} \right] \quad (3.3)$$

where  $\ell = 0, 1, 2, \dots$  denotes the angular momentum quantum number. In the limiting case of a single active electron (SAE) (which is reasonable for Rydberg states), the

Hamiltonian can be written as

$$H = -\frac{\hbar^2}{2m_e} \nabla^2 + \frac{\ell(\ell+1)}{2m_e r^2} - \frac{e^2}{4\pi\epsilon_0} \frac{Z}{r} \quad (3.4)$$

In Chapter 5, the radial equation of the Schrödinger equation is solved, including the above Hamiltonian in a radially symmetric potential, thus the Coulomb potential,  $\frac{e^2}{4\pi\epsilon_0} \frac{Z}{r}$ , is replaced by the spherically symmetric potential of  $C_{60}$ ,  $V(r)$ , as written in Eq. 4.4, giving

$$\left[ \frac{\hbar^2}{2\mu} \left( -\nabla^2 + \frac{\ell(\ell+1)}{r^2} \right) + V(r) \right] \psi_{n_{jellium},\ell}(r) = E_{n_{jellium},\ell} \psi_{n_{jellium},\ell}(r) \quad (3.5)$$

where  $\ell = 0, 1, 2, \dots$  denotes the angular momentum quantum number,  $\mu$  the reduced mass, and  $E_{n_{jellium},\ell}$  is the energy eigenvalue, with  $n_{jellium} = 1, 2, \dots$  indicating one more than number of nodes ( $n_{jellium} = N + 1$ ) of the bound state wavefunction.

For more sophisticated calculations, density functional theory (DFT) is presently a popular approach to the  $C_{60}$  problem. DFT considers the density of the electronic system rather than each individual electron, thereby reducing the number of parameters from  $3N$  to  $3$ . Two recent theoretical for  $C_{60}$  use DFT. The first uses a time-dependent density functional theory (TDDFT) with an ionic background treated as jellium model [BCM01]. The second work uses a density-functional-based tight-binding electron-ion dynamics (DFTED) [TNE01]. The results from these works are used in the interpretation of the experimental results, however, a detailed explanation of these calculations is beyond the intention of this work.

### Single Active Electron vs. Multiple Active Electrons

Almost all atoms, molecules, and clusters have more than one electron. Exact quantum mechanical solutions of strong field-matter interaction are presently not feasible beyond simple atoms of at most two electrons, therefore it is necessary to implement approximations.

One common approximation to simplify the problem is to consider a single active electron (SAE)<sup>1</sup>. This assumes that the electric field solely interacts with the lowest bound electron. In other words, after the lowest bound electron is promoted to an excited state, the probability that the excited electron will be further excited or

---

<sup>1</sup>A crude approximation even in relatively low electric fields, this approximation completely fails at high fields where tunnelling ionization occurs.

ionized is greater than exciting a second electron. SAE has been used to successfully describe sequential ionization processes. However, this approximation neglects the dynamics of the remaining bound electrons, which are important for large systems with delocalized electrons, particularly in strong external fields.

A second common approximation is the strong field approximation (SFA), which assumes that the strong electric field drives the continuum electrons and that Coulomb interaction with the core is negligible.

As the complexity of the molecule and the laser intensity is increased, the SAE approximation is no longer valid and thus the electrons can no longer be considered independently. Recent experimental [MSR03, LBI02] and theoretical [BCM01, FKM03] work has indicated that for larger systems in moderate laser intensity multiple active electrons (MAE) are excited. A discussion of SAE versus MAE will be continued throughout this work.

## 3.2 Strong Field Phenomena

Strong electric fields affect the motion of the electrons thus distorting the electronic levels (or the energy eigenvalues). There are several phenomena which occur during an intense laser pulse which must be considered in the interpretation of experimental results : AC Stark shift, Ponderomotive potential, and Keldysh parameter.

The term “strong electric field” is dependent on the properties of the molecular system as well as the frequency of the exciting electric field. In this section, brief descriptions are made for several important field induced phenomena.

### 3.2.1 AC Stark Shift

The shifting (or splitting) of spectral lines due to an external electric fields is called the Stark effect. The external electric field creates a perturbation to the quantum system, shifting the energy eigenvalues. Qualitatively, the electric field deforms the unperturbed electronic orbitals (induces a polarization) of the atom (or molecule) with which the electric field then interacts.

The external electric field is usually considered under perturbation theory. The first order perturbation is dependent on the electric dipole,  $\mathbf{d} \equiv -e\mathbf{r}$ , and the second order perturbation is dependent on the polarizability,  $\alpha$  (introduced in Eq. 3.8). The

energy eigenvalue of a quantum state in an external electric field can be written as

$$E \simeq E_{nlm} + \langle nlm | -\mathbf{d} \cdot \mathcal{E} | nlm \rangle + \sum_{n',l',m' \neq n,l,m} \frac{|\langle n'l'm' | -\mathbf{d} \cdot \mathcal{E} | nlm \rangle|^2}{E_{nlm} - E_{n',l',m'}} \quad (3.6)$$

where  $E_{nlm}$  is the unperturbed eigenenergy,  $\mathcal{E}$  is the electric field, and  $|n, l, m\rangle$  denotes the quantum wavefunction. Here, only the first two orders of correction are considered.

Considering a linearly polarized laser (along the  $z$  axis), the electric field of a laser can be considered as  $\mathcal{E}_z = \mathcal{E} \cos \omega t \hat{\mathbf{z}}$ . The time dependent change in energy,  $\Delta E(t)$  can be expressed as the sum of the first and second order perturbation.

$$\Delta E(t) = -e\mathcal{E} \cos \omega t \langle nlm | z | nlm \rangle - e^2 \mathcal{E}^2 \cos^2 \omega t \sum_{n',l',m' \neq n,l,m} \frac{|\langle n'l'm' | z | nlm \rangle|^2}{E_{n'l'm'} - E_{n,l,m}} \quad (3.7)$$

where  $z$  is the magnitude along the  $z$ -axis,  $\omega$  is the frequency of the laser, and  $t$  is the time. The first term is the linear Stark shift, which will vanish due to symmetry reasons. The quadratic Stark effect has a time average of  $1/2$ , thus the shift in energy can be written as

$$\Delta E(t) = -\frac{1}{2} e^2 \mathcal{E}^2 \cos^2 \theta \sum_{n',l',m' \neq n,l,m} \frac{|\langle n'l'm' | z | nlm \rangle|^2}{E_{nlm} - E_{n',l',m'}} = -\frac{1}{4} \alpha \mathcal{E}^2 \quad (3.8)$$

However, this is only correct when the degeneracy is lifted. The electric field of a laser is oscillatory, which gives rise to the AC Stark effect or dynamic Stark effect. Each individual energy eigenvalue is changed by different amounts depending on the polarizability of the level. The optical polarizability of the ground state of  $C_{60}$  has been found to be  $\alpha = 79 \text{ \AA}^3$  at 1064 nm [BBL00]. Assuming a laser intensity of  $3.5 \cdot 10^{12} \text{ W/cm}^2$ , the shift in the ground state corresponds to 0.362 eV. The polarizabilities of higher excited states of  $C_{60}$ , which are less separated energetically, are not known, but according to Eq. 3.8 they can be expected to be larger, since  $E_{nlm} - E_{n'l'm'}$  becomes smaller.

It should be noted that the perturbation theory in extremely high electric fields is most likely invalid, and thus the first order might not be neglected since the degeneracy would not be lifted.

### 3.2.2 Ponderomotive Potential

The ponderomotive potential describes the average oscillation energy that is acquired by a free electron in the radiation field. It is given by the equation

$$U_p = \frac{e^2}{2m_e\epsilon_0 c\omega_L^2} I \quad (3.9)$$

where  $m_e$  is the mass of the electron,  $\omega_L$  is the angular frequency of the laser irradiation,  $I$  is the intensity,  $e$  is the electric charge,  $\epsilon_0$  is the dielectric constant, and  $c$  is the speed of light. The ponderomotive potential is dependent on the square of the wavelength and linearly dependent on intensity, this can be numerically expressed as

$$U_p = 9.34 * \lambda^2[\mu m] I[10^{14} W/cm^2] \quad (3.10)$$

For a central wavelength of 800 nm and a peak intensity of  $5*10^{13}$  W/cm<sup>2</sup>, the ponderomotive potential is 2.99 eV. In other words, it is nearly equivalent to the energy of two 800 nm photons.

### 3.2.3 Keldysh Parameter

The Keldysh parameter is a frequently used parameter to describe the laser interaction with matter (particularly atoms) in order to distinguish between the strong and weak field regimes. This parameter was introduced by Keldysh in 1965 [Kel65] and is

$$\gamma = \sqrt{\frac{IP}{2U_p}} = \sqrt{\frac{IP\epsilon_0 m_e c\omega_L^2}{e^2 I}} \quad (3.11)$$

Assuming  $\hbar\omega < IP$ , the weak field regime occurs when  $\gamma > 1$ , i.e., where the field strength is weaker than the IP and multi-photon ionization is the dominant process for removing an electron. For  $\gamma \ll 1$ , the field is stronger than the ionization potential. This is the strong field regime and corresponds to where tunneling ionization or barrier suppression ionization is the dominant process.

The barrier between strong and weak field physics can be defined when the ponderomotive potential is equal to the ionization potential [HLS05]. For C<sub>60</sub>, with an ionization potential of 7.59 eV, a critical intensity of  $1.3*10^{14}$  W/cm<sup>2</sup> is found. In general, this intensity is higher than the experiments performed in the present work

and thus the results can be discussed in the MPI and ATI regime<sup>2</sup>.

The Keldysh parameter can also be considered as the ratio between the time necessary to cross the barrier (when suppressed),  $t_{tunnel}$ , and the period of the exciting laser field,  $t_L$ . The weak regime corresponds to the situation where the tunnelling time is long in comparison to the electric field ( $t_{tunnel} > t_L$ ).

### 3.3 Ionization of Molecules

Two types of ionization can be defined: direct, which is the emission of an electron during the laser pulse, and delayed, which is emission after the electric field of the laser has passed.

Direct ionization is a result of absorption of enough photons to cross the ionization potential (Single or Multi-Photon Ionization) or electrons which escape as the potential barrier is suppressed in the strong external electric field.

Statistical ionization is the statistical emission of an electron from either a hot electronic system or a highly vibrationally excited system. This occurs in systems where the ionization potential is comparable or lower than the dissociation barrier, e.g. in C<sub>60</sub>.

#### 3.3.1 Direct Ionization

##### Multiphoton Ionization / Above threshold ionization ( $\gamma > 1$ )

At low light intensity, the removal of an electron is achieved when the energy of a photon,  $E_p = \hbar\omega$  exceeds the ionization potential. The observation of a strong wavelength dependence yet a weak intensity dependence was the basis of the photoelectric effect, discovered by Einstein in 1905.

However, at higher intensities, the absorption of multiple photons becomes possible and may lead to ionization. Multiphoton ionization (MPI) is condition where the absorption of several photons is necessary to surpass the ionization potential. In

---

<sup>2</sup>Two measurements of the angular distribution of photoelectrons used intensities at or above the critical threshold. However, these results are not used in the discussion of excitation mechanisms of C<sub>60</sub>

direct MPI, no intermediate states are involved, and the ionization rate is given by

$$S = \sigma_n I^n \Rightarrow \log S = n \log \sigma_n I \quad (3.12)$$

where  $S$  is the signal,  $n$  is the number of photons absorbed,  $I$  is the intensity, and  $\sigma_n$  is the absorption cross-section for an  $n$ -photon process. The value of  $n$  is often determined by plotting  $\log S$  versus  $\log I$  and fitting the slope [DKr00]. This model is acceptable for atoms, but is questionable for larger systems [HHC03].

When intermediate states are resonantly excited, the slope will be altered from a pure direct transition by lowering the order of the intensity dependent step. This process is known as resonance enhanced multi-photon ionization (REMPI). Field induced - REMPI (FIREMPI) indicates that the electronic states will be shifted into resonance by the strong external electric field, e.g. through the AC-Stark shift.

When the number of photons absorbed exceeds the minimum number,  $n$ , required for ionization by  $s$ , the process is termed as above threshold ionization (ATI). The energies of the emitted electron are given by

$$E_{el} = (n + s)\hbar\omega - IP \quad (3.13)$$

where  $\hbar\omega$  is the photon energy and  $IP$  is the ionization potential. This is easily characterized by equally spaced peaks in photoelectron spectra corresponding to the photon energy.

### **Tunnelling Ionization / Barrier Suppression Ionization ( $\gamma \ll 1$ )**

As the intensity is further increased, the potential energy surfaces of an atom or molecule are suppressed to the point, where an electron can tunnel through the potential barrier. Ionization that proceeds in this manner is termed ‘‘Tunnelling ionization’’. The probability depends on both the amplitude and frequency of the electric field. The probability of tunnelling can be calculated through ADK formalism [ADK86] which has been developed for neutral as well as multiply charged atoms.

The tunnelling regime (or strong field regime) begins when the Keldysh parameter,  $\gamma$  is much smaller than 1 ( $\gamma \ll 1$ ). This corresponds to the situation where the ponderomotive potential is nearly equivalent to the ionization potential.

At even higher intensities, the laser electric field suppresses the potential energy surface so far that electrons are able to escape freely from the molecule. This is called ‘‘Barrier Suppression Ionization’’ (BSI)

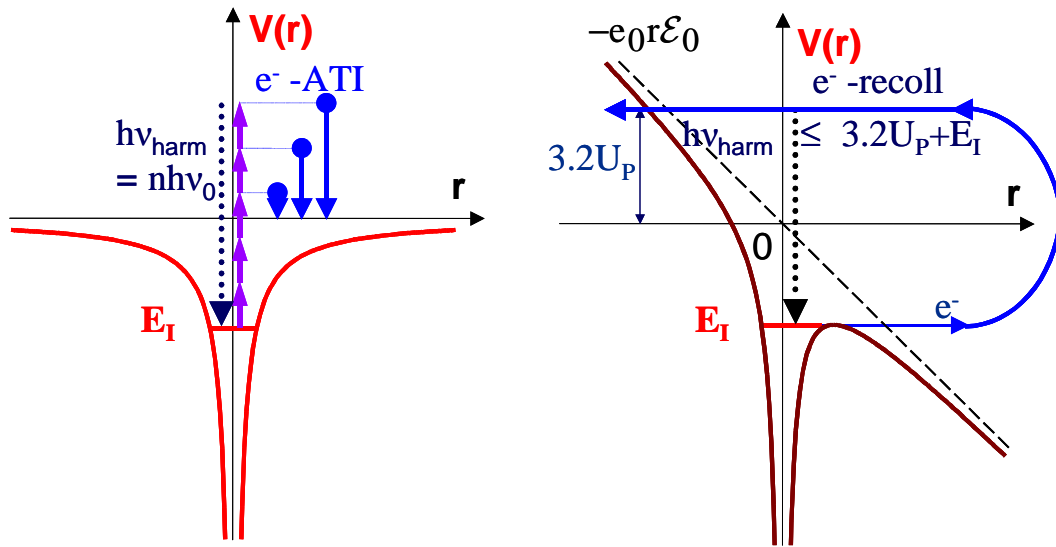
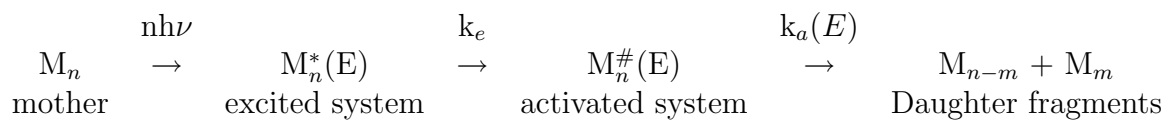


Figure 3.1: Schematic illustration of two ionization processes of atoms in strong fields. Left: Multiphoton ionization, which occurs in a weak field regime, where the atomic potential is not significantly distorted. Above threshold ionization also proceeds. Right: Tunnelling regime, also known as above the barrier ionization, indication is shown for electronic recollision (linear polarization), with maximum recollision energy of  $3.2 U_p$ . From [HLS05].

### 3.4 Molecular Fragmentation

Fragmentation or dissociation of molecules or clusters is one mechanism of energy relaxation. Unimolecular fragmentation occurs when there is a separation of the whole into two or more parts. The initial molecule is typically called the mother and the fragments are called daughters. Fragmentation and dissociation concerns the neutral emission of particles. Fission describes the event when two charges separate. Unimolecular fragmentation can be schematically written as:



where  $M_n(E)$  denotes the energized system and  $M_n^\#(E)$  denotes the activated state, which is an intermediate state between product and reactant. The time constant,  $k_e$ , is the time for intramolecular energy redistribution, and  $k_a(E)$  is the energy dependent time constant for activation.

Fragmentation can, in principle, proceed when the internal vibrational energy is greater than the dissociation energy. This can be separated into two different

processes, a direct, non-statistical fragmentation or statistical fragmentation.

### 3.4.1 Direct (Non-statistical) Fragmentation

Direct fragmentation can be defined as fragmentation which occurs along a well defined reaction coordinate. This is one example of non-statistical fragmentation, which can be more generally defined as fragmentation which occurs when the internal energy is not equally distributed among all degrees of freedom. This can be achieved by fragmentation on a time scale shorter than the energy redistribution time scale or excitation of a particular mode or repulsive potential energy curve.

A direct fragmentation can be envisioned when a molecule is excited to a dissociative state, and proceeds to fragment along a well defined reaction coordinate. Typically, theoretical models are needed to prove that the fragmentation indeed occurs along one reaction coordinate.

Another non-statistical fragmentation occurs when one particular vibrational mode is driven, until the amplitude of the vibration leads to dissociation. This can be achieved either by radiation tuned to the vibrational frequency or in the temporal domain by exciting a molecule with a train of well timed pulses (impulsive stimulated Raman excitation).

In large systems, such as  $C_{60}$ , numerous excited electronic states and conical intersections exist through which non-adiabatic transitions between different potential energy surfaces can occur. These transitions can occur on ultrafast timescales and may lead to a dissociative state. However, the complexity of large systems, hinders the ability to follow the system through these transitions.

### 3.4.2 Statistical Fragmentation

Several models exist to describe statistical unimolecular fragmentation and determine the rate constants at which the reaction proceeds. Three of these have been used often in literature concerning fullerenes: RRK(M), detailed balance, and evaporative ensemble.

## RRK(M)

Early theories were developed with the activation mechanism coming from collisions. Lindemann was one of the pioneers which has formed the basis of unimolecular reactions today. In this theory, the activation rate and deactivation rate is related to the rate of collisions. The fragmentation of the activated molecule was assumed to not proceed immediately, but on time scales significantly longer than the deactivation rate.

The Lindemann theory has been improved several times, most notably by Ramsperger, Rice, and Kassel [RRa27, RRa28, Kas28a, Kas28b], who have developed in the late 1920s a unimolecular reaction theory which was further extended in the 1950s by Marcus [Mar52]. In their theory, the rate of reaction is determined by the amount of internal energy, which is divided over all vibrational degrees of freedom. Statistical mechanics are used to calculate the probability of one mode containing enough energy to dissociate. This leads to the classical Ramsperger, Rice, and Kassel (RRK) equation

$$k(E, D) = A \left( \frac{E - D}{E} \right)^{s-1} \quad (3.14)$$

where  $A$  is a proportionality constant,  $E$  is the internal energy of a molecule,  $D$  is the dissociation energy, and  $s$  is the vibrational degrees of freedom. The  $A$  parameter in Eq. 3.14 can be rewritten with the reaction degeneracy,  $\alpha$  and the average vibrational frequency,  $\bar{\nu}$  as shown in Eq. 3.15

$$k(E, D) = \alpha \bar{\nu} \left( \frac{E - D}{E} \right)^{s-1} \quad (3.15)$$

For the  $C_2$  emission from  $C_{60}$ , the reaction degeneracy,  $\alpha$  is equal to 30. RRK theory predicts strict adherence to the Arrhenius equation.

RRKM uses two new aspects in comparison to RRK theory, the first is that the energisation rate,  $k(e)$ , is calculated as a function of energy with a quantum-statistical-mechanical treatment. Secondly, the calculation of  $k_a(E^*)$  is done through canonical transition state theory [HPR96]. The conversion from  $M^*$  to products is considered in terms of translation along a reaction coordinate.

## Detailed Balance

A second theoretical model for description of particle emission has been termed detailed balance, which is a highly useful model because its universality. This formalism

was developed by Weisskopf for particle emission from nuclei [Wei37] and has recently been successfully used for description of thermionic emission and fragmentation of clusters [ABH02, TAH03].

The basic tenet of this model is that for a system in equilibrium, the rate constant of the decay is related to the rate constant of the formation by the ratio of the level density of states of the parent and the product.

$$k_d \rho_P = k_{fo} \rho_d \quad (3.16)$$

where  $\rho_P$  and  $\rho_d$  are the level densities of parent and fragment and  $k_d$  and  $k_{fo}$  are the rate constants for fragmentation and capture, respectively. Only the electronic and vibrational states need to be considered for the level densities [ABH02].

The rate constant of formation is related to the cross section by

$$k_{fo} = \nu_{fo}(\sigma(\epsilon)) \frac{\rho_d(E - E_i)}{\rho_P(E)} \quad (3.17)$$

where  $\rho_d$  is the level density of the daughter,  $\rho_P$  is the level density of the parent, and  $\nu_{fo}$  is proportional to the cross section for attachment [ABH02].

A general detailed balance rate constant (without angular momentum conservation) has been determined for the unimolecular dissociation of spherically symmetric clusters [Han04].

$$k(E, \epsilon) = \frac{g\mu}{\pi^2 \hbar^3} \sigma(\epsilon) \epsilon \frac{\rho_d(E - D - \epsilon)}{\rho_P(E)} \quad (3.18)$$

where  $\epsilon$  is the kinetic energy release,  $g$  is the degeneracy,  $\mu$  is the reduced mass,  $\sigma(\epsilon)$  is the reverse cross section,  $\rho_d$  is the density of states of the daughter, and  $\rho_p$  is the density of states of the parent.

Including angular momentum, a correction term is needed [Han04]. However, this will not be considered here in this brief general introduction.

When  $\epsilon$  is small in comparison to the total energy, the level density of the daughter can be factored as

$$\rho_d(E - D - \epsilon) \approx \rho_d(E - D) \exp(-\epsilon/k_B T_m) \quad (3.19)$$

where  $k_B$  is Boltzmann's constant and  $T_m$  is the microcanonical temperature and is defined as

$$\frac{1}{k_B T_m} \equiv \frac{d}{dE} (\rho_d(E - D)) \quad (3.20)$$

The rate constant (Eq. 3.18) can be rewritten as

$$k(E, \epsilon) = \frac{g\mu}{\pi^2 \hbar^3} \sigma(\epsilon) \epsilon e^{-\epsilon/k_B T_m} \frac{\rho_d(E - D)}{\rho_P(E)} \quad (3.21)$$

This leads to an Arrhenius type formula for the dissociation [TAH03].

$$k_d(T) = A_d \exp\left(-\frac{E_d}{k_B(T - E_d/2C)}\right) \quad (3.22)$$

where  $C$  is the heat capacity and is equal to 0.0147 eV/K,  $k_d(T)$  is the temperature dependent rate constant, and  $E_d$  is the dissociation energy (see Table 3.2 for values).  $A_d$  was found to be  $3.4 \times 10^{21} \text{ s}^{-1}$  for  $\text{C}_{60}$  [TAH03].

### 3.4.3 Kinetic Energy Release Distribution

The following discussion on kinetic energy release concerns only statistical fragmentation channels. The fragmentation of a system will produce a velocity distribution for each fragment, since some of the excess internal energy released will be released as kinetic energy pushing the fragments away from each other. The kinetic energy release (KER) distribution can yield information concerning ion structures, reaction energetics, and dynamics.

The KER always has a distribution, even when the molecules are energy selected, and this distribution can be Maxwell-Boltzmann like, to which a “temperature” can be assigned. The “temperature” can be expressed through the microcanonical temperature [ABH01, ABH03].

Fragmentation products can be grouped into two groups: those with a reaction barrier and those without a reaction barrier. Exemplary potential energy surfaces for each type are shown in Fig. 3.2.

$E_A$  is the activation energy necessary to induce the dissociation process,  $D_{IorII}$  indicate the dissociation energy, and  $\epsilon$  is the KER. The potential energy surface for type I is typical for dissociations by bond cleavages, has no (or very small) reverse activation barrier, and results in low KER. Another characteristic of type I dissociation is that the KER is centered close to 0 eV. The type II potential energy surface is typical for dissociations which require a reorientation (isomerization), a reverse activation barrier exists, and there is a large KER.

$\text{C}_{60}$  has been found to have no reverse activation barrier [RHR90] and thus falls under the type I dissociation. The kinetic energy release of metastable  $\text{C}_{60}^+$  has been

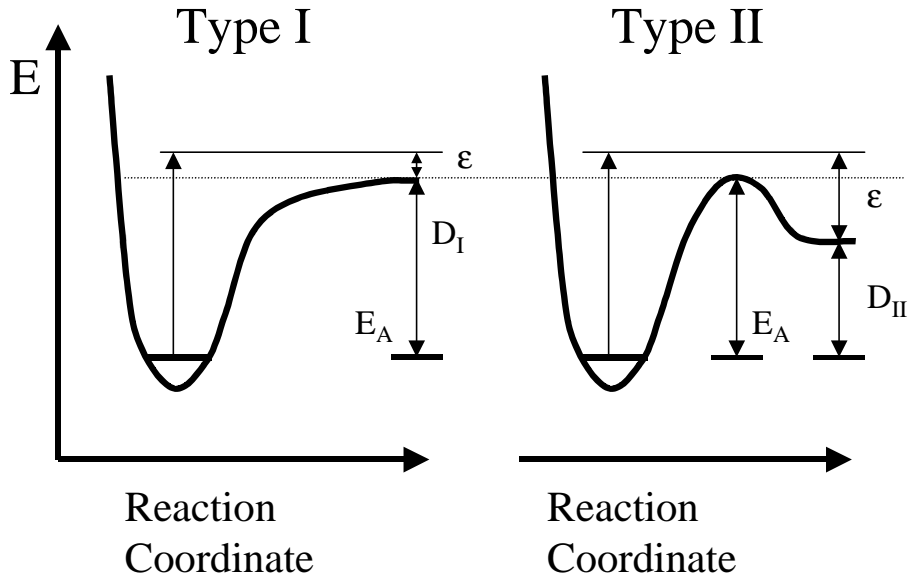


Figure 3.2: The potential energy surface along a given reaction coordinate is found to affect the kinetic energy release. Type I : Potential energy surface gradually approaches the dissociation threshold and results in a small kinetic energy release. Type II : The activation barrier lies higher in energy than the dissociated fragments (a reverse activation barrier exists).  $C_{60}$  belongs to Type I [RHR90]. Figure adapted from [LLi01].

extensively studied (see [MES01, Lif00] and references therein) and the KERD is found to be well modelled by the distribution

$$f(\epsilon) = \epsilon^{1/2} e^{-\epsilon/k_B T^\#} \quad (3.23)$$

where  $\epsilon$  is the KER and  $T^\#$  is the transition state temperature [GME04a]. Under the formalism of detailed balance, this can also be expressed as

$$f(\epsilon) \propto \epsilon \sigma(\epsilon) e^{-\epsilon/k_B T^\#} \quad (3.24)$$

where  $\sigma(\epsilon)$  is the capture cross section for the reverse reaction. The cross section for  $C_{60}$  is found to be modelled by Langevin cross section. The average KER of the metastable fragmentation channel has been found to be  $\bar{\epsilon} \simeq 0.4eV$  [Lif00].

### 3.5 The Molecule $C_{60}$

This section provides a brief overlook to some of the special properties of  $C_{60}$ . The bible of fullerene science is [DDE96], however, there has been a lot of progress in the

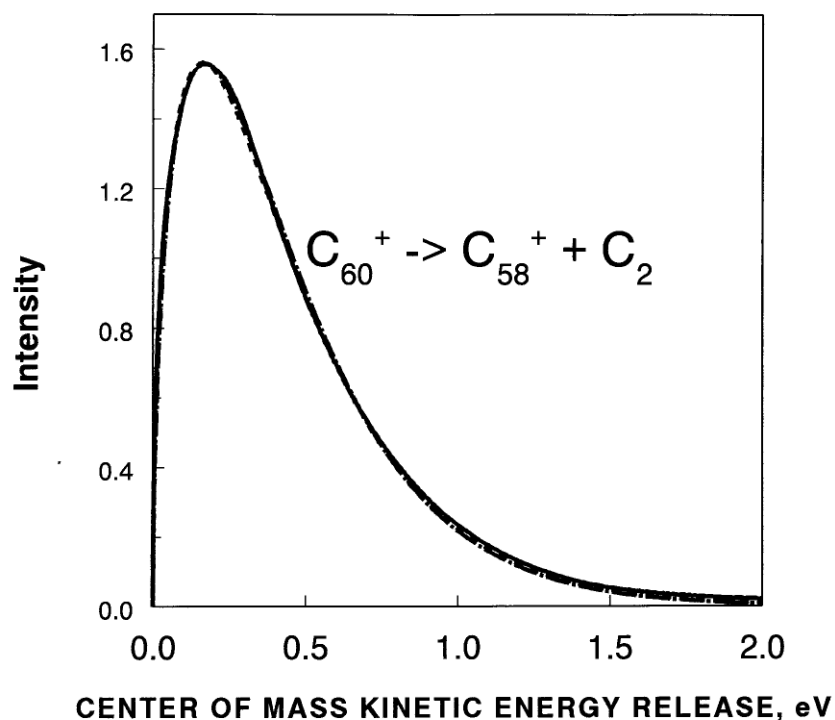


Figure 3.3: *Kinetic energy release distribution of  $C_{60}^+ \rightarrow C_{58}^+ + C_2$ . Solid line: experimental KERD. From [Lif00].*

field since 1996. The structure, electronic properties, vibrational modes, and decay mechanisms will be discussed.

### 3.5.1 Geometric Structure

Carbon is one of the most abundant elements and exists in four allotropic forms: amorphous carbon, graphite, diamond, and fullerenes. Carbon's tetravalent outer shell allows it to easily bond with other atoms or with itself. The carbon clusters have two properties distinguishing them from other clusters. The first is that the clusters are covalently bound, in comparison to the more weakly bound Van-der-Waals clusters. The second characteristic is that for carbon clusters larger than 30 carbon atoms only even numbered clusters are formed.

Carbon clusters up to the size of 9 have been found to have a linear structure. Clusters that are between 10 and 30 carbon atoms have a ring structure. Beyond 30 carbon atoms exist the fullerenes. These three dimensional structures consist of

rings of pentagons and hexagons.

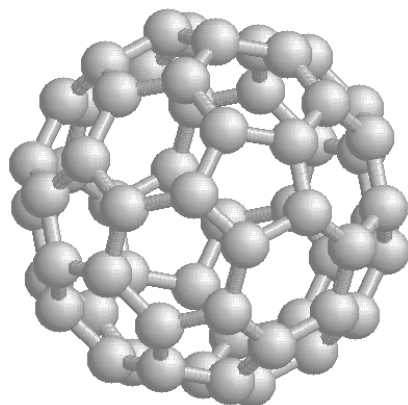


Figure 3.4: *Picture representing the unique structure of  $C_{60}$ .*

The  $C_{60}$  cluster was discovered to be particularly stable in comparison to its neighbors, and it was suggested that the stability was a result of a closed cage structure [KHB85]. The cage is made of 12 pentagons and 20 hexagons, representing a miniature soccer ball with a 7.1 Å diameter. It is the smallest cage structure which has no neighboring pentagons. The  $C_{60}$  cluster belongs to the  $I_h$  point group, which is a truncated icosahedron, and means that all atoms are equivalent. The unique structure of  $C_{60}$  is shown in Fig. 3.4.

### 3.5.2 Ionization Potentials and Dissociation Energies

The ionization potential and dissociation energy are two fundamental properties that characterize a molecule.  $C_{60}$  is an unusual molecule in that the dissociation energy of a  $C_2$  unit is larger than the ionization potential.

The first ionization potential of  $C_{60}$  has been experimentally found to be  $7.59 \pm 0.02$  eV by single photon ionization. Higher ionization potentials increase roughly linearly, with the second and third ionization potential being  $11.4 \text{ eV} \pm 0.04 \text{ eV}$  [SVK92] and  $16.6 \text{ eV} \pm 1.0 \text{ eV}$  [SDW94], respectively. The first ionization potentials for neighboring fullerenes are about 0.5 eV lower in magnitude [ZEB91, Cam03].

The absolute value of the dissociation energy of  $C_{60}$  has been debated for many years, with typically the theoretical values higher than experimental values. The discrepancy for many of the experimental works is due to the unknown Arrhenius

pre-exponential value, which is dependent on the competition between different cooling channels. The most recent dissociation energy found in literature is  $11.2 \pm 0.2$  eV [GME04b]. However, it should be mentioned that through a different measurement technique another group has found the dissociation energy of neutral C<sub>60</sub> to be  $10.8 \pm 0.3$  [TAH03]. A second paper from this group [TAG01] details the binding energies for singly charged C<sub>60</sub> and will be used later in this work. For consistency, all dissociation energy values presented in Table 3.2 will come from the Märk group [MES99b, GME04b]. The error bars (not listed) are of magnitude 0.2 eV to 0.4 eV and are a result of the statistical uncertainty of the measurement [GME04b]. The error bars do not take into account systematic errors, such as their assumption of Arrhenius pre-exponential factor. The theoretical values are taken from [DAM03].

Two features should be pointed out. First, the relative dissociation energy of C<sub>60</sub> is around 1 eV higher than the neighboring fullerene structures, indicating the particularly stable structure. Secondly, the dissociation energy for a particular fragment is found to be charge independent [TAG01, MES99b, DAM03].

Table 3.1: *Several important parameters of C<sub>60</sub>. The ionization energies and dissociation energies are particularly important for understanding the interaction of C<sub>60</sub> with fs-laser radiation.*

Property	Value	Source
Symmetry	I <sub>h</sub>	[KHB85]
Mean ball diameter	7.1 Å	[DDE96]
First IP	7.59 eV	[SHH95]
Second IP (IP of C <sub>60</sub> <sup>+</sup> )	11.4 eV	[SVK92]
Third IP (IP of C <sub>60</sub> <sup>++</sup> )	16.6 eV	[SDW94]
Dissociation Energy C <sub>60</sub> (experiment)	$11.2 \pm 0.2$ eV	[GME04b]
Dissociation Energy C <sub>60</sub> (theory)	11.37 eV	[DAM03]

Table 3.2: *Dissociation energies for different fragmentation steps. Experimental dissociation energy values are from [GME04b](neutrals and single charged) and [MES99b](double charged), theoretical values from [DAM03]. Error bars for experimental values are between 0.2 and 0.4 eV and result from statistical uncertainty in the authors measurement [GME04b].*

$\Delta N$	Notation	$D_{60-2(\Delta N-1)}$ [eV]	Theory[eV]
1	$C_{60} \rightarrow C_{58}$	11.2	11.37
2	$C_{58} \rightarrow C_{56}$	9.7	8.12
3	$C_{56} \rightarrow C_{54}$	9.9	8.48
4	$C_{54} \rightarrow C_{52}$	9.7	8.44
5	$C_{52} \rightarrow C_{50}$	8.9	7.89
6	$C_{50} \rightarrow C_{48}$	9.75	
7	$C_{48} \rightarrow C_{48}$	9.6	
1	$C_{60}^+ \rightarrow C_{58}^+$	10.7	10.64
2	$C_{58}^+ \rightarrow C_{56}^+$	9.9	8.35
3	$C_{56}^+ \rightarrow C_{54}^+$	10.1	8.43
4	$C_{54}^+ \rightarrow C_{52}^+$	9.6	8.38
5	$C_{52}^+ \rightarrow C_{50}^+$	9.0	8.10
6	$C_{50}^+ \rightarrow C_{48}^+$	9.9	
7	$C_{48}^+ \rightarrow C_{46}^+$	9.6	
1	$C_{60}^{++} \rightarrow C_{58}^{++}$	10.6	10.19
2	$C_{58}^{++} \rightarrow C_{56}^{++}$		8.46
3	$C_{56}^{++} \rightarrow C_{54}^{++}$		8.55
4	$C_{54}^{++} \rightarrow C_{52}^{++}$		7.96
5	$C_{52}^{++} \rightarrow C_{50}^{++}$		8.57

### 3.5.3 Electronic Structure

The electronic structure of a molecule is one key to understanding the absorption of energy from laser radiation. The energy spacing between electronic levels indicates the number of photons needed to excite an electron to the upper level and the electronic symmetry defines whether the excitation is allowed.

The valence structure of C<sub>60</sub> is composed of 180  $\sigma$  orbitals and 60  $\pi$  orbitals. The  $\sigma$ -orbitals lie 3 - 6 eV below the Fermi level and bond the atoms together. The remaining 60 electrons are in delocalized  $\pi$  orbitals that are oriented perpendicularly to the surface of the C<sub>60</sub> spherical shell. These  $\pi$  orbitals lie close to the Fermi level and define the electronic structure.

The highest occupied molecular orbital (HOMO) level has the total electronic symmetry of  ${}^1A_g$  and has the angular momentum  $\ell = 5$ . The lowest unoccupied molecular orbital (LUMO) level has  ${}^1T_{1g}$  symmetry and is therefore an optically forbidden transition. The LUMO+1 level has the  ${}^1T_{1u}$  symmetry and is the lowest optically allowed transition at 3 eV. Fig. 3.5 indicates these levels on a single electron energy level diagram. On the left hand side of Fig. 3.5, two absorption spectra are shown. The dotted line represents measurements in the gas phase, while the solid line indicates a measurement in a hexane solution.

The delocalized electrons of C<sub>60</sub> lead to the possibility of a correlated excitation of many electrons. Single photon excitation has evidenced a giant plasmon resonance centered at 20 eV [HSV92]. The excitation of multiple electrons may also be possible with strong laser fields, as will be discussed in this thesis.

### 3.5.4 Vibrational Properties

There are  $60 \times 3 - 6 = 174$  vibrational modes of C<sub>60</sub>, of which there are 46 distinct vibrational modes. These can be expressed as

$$\begin{aligned} \Gamma_{C_{60}} = & 2A_g[1] + 3F_{1g}[3] + 4F_{2g}[3] + 6G_g[4] + 8H_g[5] \\ & + A_u[1] + 4F_{1u}[3] + 5F_{2u}[3] + 6G_u[4] + 7H_u[5] \end{aligned} \quad (3.25)$$

where the symmetry labels refer to the irreducible representations of icosahedral symmetry and the subscripts  $g$  and  $u$  refer to the symmetry of the eigenvector upon inversion [DDE96]. The numbers in brackets indicate the degeneracy of each state.

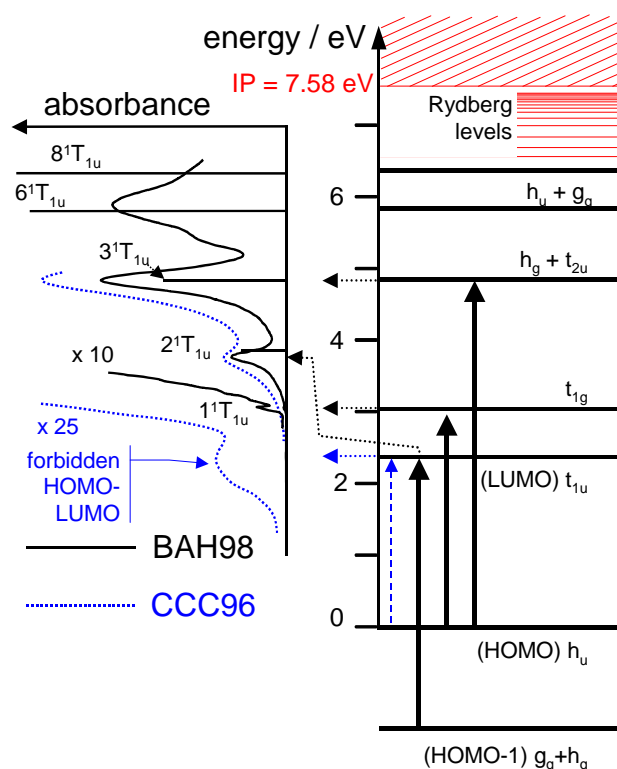


Figure 3.5: *Electronic absorption spectra (left) and single electron energy diagram (right). Figure taken from [HLS05], experimental data from [BAH98, CCC96].*

In the ground state, there are 10 Raman active modes,  $2 A_g + 8 H_g$ , and 4 infrared active modes,  $4 F_{1u}$ . The remaining 32 vibrational modes are optically “silent”. The optically active modes are listed in Table 3.3 along with their experimental frequency and vibrational period.

In the context of this work, the most important modes to consider are the  $A_g(1)$ ,  $A_g(2)$ , and the  $H_g(1)$  vibrational modes. The  $A_g(1)$  mode is the symmetric breathing mode, in which all atoms move radially outward with an equal amplitude. Calculations have shown that this mode to be excited under high intensity, short laser pulse duration [TNE01, ZSG03]. The  $A_g(2)$  mode is the pentagonal pinch mode and has also been found to be excited with the the interaction of  $C_{60}$  with 10 fs laser radiation of slightly lower fluence ( $0.006 \text{ mJ/cm}^2$ ) [TNE01]. The  $H_g(1)$  mode corresponds to an elongation of one axis of the sphere, for example, along the laser polarization.

The vibrational modes of electronically excited  $C_{60}$  are not precisely known. The excitation of an electron weakens the bonds between carbon atoms. This weakening affects the vibrational frequencies, but for the vibrational modes of  $C_{60}$  this is a

Table 3.3: *Optically active vibrational modes. Experimental values have been found by fits of Raman [DZH93] and IR spectra [WRE93] of thin films. A summary of all modes can be found in [DDE96].*

	experimental frequency [cm <sup>-1</sup> ]	vibrational period
Raman Active modes		
A <sub>g</sub> (1)	497.5	67 fs
A <sub>g</sub> (2)	1470.0	23 fs
H <sub>g</sub> (1)	273.0	122 fs
H <sub>g</sub> (2)	432.5	77 fs
H <sub>g</sub> (3)	711.0	47 fs
H <sub>g</sub> (4)	775.0	43 fs
H <sub>g</sub> (5)	1101.0	30 fs
H <sub>g</sub> (6)	1251.0	27 fs
H <sub>g</sub> (7)	1426.5	23 fs
H <sub>g</sub> (8)	1577.5	21 fs
IR Active modes		
F <sub>1u</sub> (1)	526.5	63 fs
F <sub>1u</sub> (2)	575.8	58 fs
F <sub>1u</sub> (3)	1182.9	28 fs
F <sub>1u</sub> (4)	1429.2	23 fs

complex problem, and thus is difficult to predict what changes would occur.

### 3.5.5 Relaxation Processes

After energy is absorbed from the laser pulse, the energy will be redistributed through processes of electron-electron coupling or electron-phonon coupling. The release of excess energy can occur through ionization, fragmentation, and photon emission. The characteristic time scales of these processes are dependent on the molecular properties.

The interaction of femtosecond laser radiation has been found to significantly different than nanosecond laser radiation. Namely, ionization is easier and fragmentation is more difficult. Generally, femtosecond excitation removes the electron prior to the fragmentation.

In Table 3.4, a list of the possible channels for  $C_{60}$  to release energy after photo-excitation. The preferred pathway is strongly dependent on the amount of excitation of the system. Short femtosecond laser pulses tend to excite the electronic system, and in the case of ATI, the electron takes away the extra energy. Since energy redistribution is a major part of this work, only a short, general presentation will be discussed here. Further details will be given in the text when necessary.

Some of these processes occur on the time scales of interest in this work or are not observed with femtosecond laser irradiation.

Radiative cooling (photon emission) is expected to play only a very minor role in the femtosecond and picosecond time domains, which is the focus of this work. Radiative cooling can proceed through fluorescence or phosphorescence. These mechanisms occur on much longer time scales ( $\mu s$ ) than the experiments.

Delayed ionization is not observed for laser pulse durations shorter than 500 fs [CHH01], indicating that ionization with shorter pulses is produced by direct ionization (either MPI or Tunneling Ionization). The delayed ionization, which takes place on the microsecond timescale, is a result of the competition between ionization and fragmentation. However, there are still several unanswered questions about this phenomena best saved for another thesis.

There are two possible fragmentation channels : sequential fragmentation and fragmentation by loss of  $C_n$ . For nanosecond laser excitation, the  $C_n$  fragmentation pathway is believed not to exist. The fragmentation of  $C_{60}$  after femtosecond laser excitation is discussed in length in Chapter 5.

Table 3.4: Possible multiphoton processes of C<sub>60</sub> Adapted from [LWu92].

$C_{60} + nh\nu$	$\rightarrow C_{60}^+ + e^-$	direct ionization
	$\rightarrow C_{60}^{**}$	photo excitation
	$\rightarrow C_{60}^{*\#}$	$\rightarrow C_{60} + h\nu$ photon emission
		$\rightarrow C_{60}^+ + e^-$ delayed ionization
		$\rightarrow C_{60}^+ + C_2$ fragmentation
		↓
		$\rightarrow C_{58}^+ + C_2$ sequential fragmentation
		↓
		$\rightarrow C_{56}^+ + C_2$ sequential fragmentation
		$\rightarrow C_{60-2n}^+ + C_{2n}$ fragmentation via C <sub>n</sub> loss